Leckie, R.M., Sigurdsson, H., Acton, G.D., and Draper, G. (Eds.), 2000
Proceedings of the Ocean Drilling Program, Scientific Results, Vol. 165

19. A COMPARATIVE STUDY OF DIAGENETIC PATHWAYS IN SEDIMENTS OF THE CARIBBEAN SEA: HIGHLIGHTS FROM PORE-WATER RESULTS[1]

Timothy W. Lyons,[2] Richard W. Murray,[3] and D. Graham Pearson[4]

ABSTRACT

Leg 165 of the Ocean Drilling Program afforded a unique opportunity to investigate organic and inorganic geochemistry across a wide gradient of sediment compositions and corresponding chemical pathways. The solid fractions at Sites 998, 999, 1000, and 1001 reveal varying proportions of reactive carbonate species, a labile volcanic ash fraction occurring in discrete layers and as a dispersed component, and detrital fluxes that derive from continental weathering. The relative proportions and reactivities of these end-members strongly dictate the character of the diagenetic profiles observed during the pore-water work of Leg 165. In addition, alteration of the well-characterized basaltic basement at Site 1001 has provided a strong signal that is reflected in many of the dissolved components. The relative effects of basement alteration and diagenesis within the sediment column are discussed in terms of downcore relationships for dissolved calcium and magnesium.

With the exception of Site 1002 in the Cariaco Basin, the sediments encountered during Leg 165 were uniformly deficient in organic carbon (typically <0.1 wt%). Consequently, rates of organic oxidation were generally low and dominated by suboxic pathways with subordinate levels of bacterial sulfate reduction and methanogenesis. The low rates of organic remineralization are supported by modeled rates of sulfate reduction. Site 1000 provided an exception to the generally low levels of microbially mediated redox cycling. At this site the sediment is slightly more enriched in organic phases, and externally derived thermogenic hydrocarbons appear to aid in driving enhanced levels of redox diagenesis at great depths below the seafloor. The entrapment of these volatiles corresponds with a permeability seal defined by a pronounced Miocene minimum in calcium carbonate concentration recognized throughout the basin and with a dramatic downcore increase in the magnitude of limestone lithification. The latter has been tentatively linked to increases in alkalinity associated with microbial oxidation of organic matter and gaseous hydrocarbons.

Recognition and quantification of previously unconstrained large volumes and frequencies of Eocene and Miocene silicic volcanic ash within the Caribbean Basin is one of the major findings of Leg 165. High frequencies of volcanic ash layers manifest as varied but often dominant controls on pore-water chemistry. Sulfur isotope results are presented that speak to secondary metal and sulfur enrichments observed in ash layers sampled during Leg 165. Ultimately, a better mechanistic understanding of these processes and the extent to which they have varied spatially and temporally may bear on the global mass balances for a range of major and minor dissolved components of seawater.

INTRODUCTION

The present synthesis is designed to draw attention to an intriguing array of geochemical findings from the pore-water study of Leg 165 while incorporating new geochemical data and interpretative methods. Leg 165 was diverse in its scientific agenda, with discoveries spanning the Cretaceous/Tertiary (K/T) boundary, records of extensive Cenozoic volcanism, multifaceted paleoceanographic considerations such as a basinwide Miocene record of abrupt diminution in carbonate accumulation, and records of the basaltic basement and their chemical relationships to the overlying sediments. The intent of the present synthesis is to provide a snapshot from the pore-water work during Leg 165 within the context of the broad agenda of the cruise. We have not attempted to integrate all the nuances of the complex systems into this report—the many details and data are available in Sigurdsson, Leckie, Acton, et al. (1997)—but rather our goal is to illustrate through representative figures and supporting text the geochemical story that unfolded during Leg 165. In doing this, we have emphasized only Sites 998, 999, 1000, and 1001, which are linked by their characteristic sedimentation rates, ash and carbonate richness, and organic deficiencies (see Fig. 1 and Sigurdsson, Leckie, Acton, et al. [1997] for site background). The rapidly accumulating, organic-rich sediments of Site 1002 in the anoxic Cariaco Basin are not discussed in the present report. The included results allow us to deconvolve complex pore-water signals derived from an abundance of reactive carbonate phases, extensive alteration of labile volcanic ash within the sediment column, strong pore-water linkages to alter-

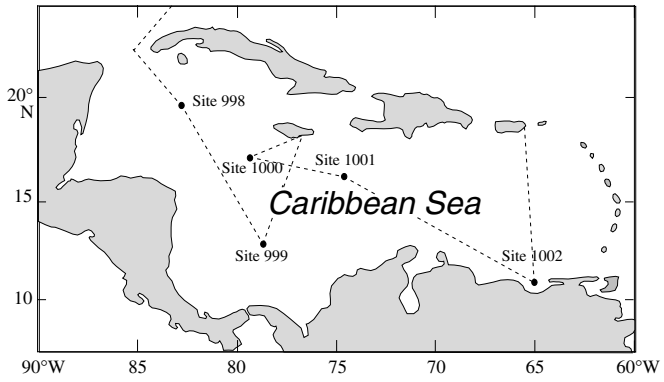

Figure 1. Site locations for ODP Leg 165. Water depths (drill-pipe measurements from sea level) for Sites 998, 999, 1000, 1001, and 1002 are 3180, 2828, 916, 3260, and 893 m, respectively. Site 998 = Cayman Rise; Site 999 = Kogi Rise (Colombian Basin); Site 1000 = Pedro Channel (northern Nicaraguan Rise); Site 1001 = Hess Escarpment (lower Nicaraguan Rise); and Site 1002 = Cariaco Basin.

[1]Leckie, R.M., Sigurdsson, H., Acton, G.D., and Draper, G. (Eds.), 2000. *Proc. ODP, Sci. Results,* 165: College Station, TX (Ocean Drilling Program).
[2]Department of Geological Sciences, University of Missouri-Columbia, Columbia, MO 65211, U.S.A. lyonst@missouri.edu
[3]Department of Earth Sciences, Boston University, Boston, MA 02215, U.S.A.
[4]Department of Geological Sciences, Durham University, Durham DH1 3LE, United Kingdom.

ation of underlying basaltic basement, and varying but low rates of biogeochemical cycling of redox-sensitive elements.

METHODS

Procedural details for core processing and the analytical approaches, with the exception of the sulfur methodologies discussed below, are provided in Sigurdsson, Leckie, Acton, et al. (1997). In brief, sulfate was determined by ion chromatography. Dissolved cations were measured using flame atomic absorption spectrometry. Alkalinity was determined by Gran titration, and inorganic carbon ($CaCO_3$) was quantified via coulometric titration. Total carbon and sulfur were measured using a Carlo Erba CNS analyzer; total organic carbon (TOC) was calculated as the difference between total and inorganic carbon. Silica, ammonium, and phosphate were quantified spectrophotometrically. Headspace gases were evaluated using gas chromatography equipped with both flame ionization and thermal conductivity detectors.

Concentrations of total reduced inorganic sulfur were measured using the chromium reduction method described by Canfield et al. (1986). Based on visual evaluations of sediment samples and discrete ash layers, it is likely that most, if not all, of this Cr-reducible sulfur represents pyrite. Isotopic compositions of bulk "pyrite" sulfur for selected ash samples were measured on Ag_2S precipitates of the sulfide liberated during chromium reduction (Lyons, 1997). Aliquots of the Ag_2S were combusted in the presence of cupric oxide under vacuum for a quantitative conversion to sulfur dioxide and analyzed via mass spectrometry. Sulfur isotope data are expressed as per mil (‰) deviations from the sulfur isotope composition of the troilite phase of the Cañon Diablo meteorite (CDT) using the conventional delta ($\delta^{34}S$) notation. Sulfur isotope results are generally reproducible within ± 0.1‰ to 0.2‰. Sulfur yields via the chromium reduction method are typically 96% or better using pyrite standards.

ORGANIC REMINERALIZATION: REDOX PATHWAYS

With the exception of Site 1002, the sites of Leg 165 were characterized by low TOC contents and, correspondingly, redox pathways dominated by suboxic diagenesis and low rates of bacterial sulfate (SO_4^{2-}) reduction, an anaerobic process (Froelich et al., 1979). These reactions are recorded as enrichments in dissolved manganese and iron in the upper sediment layers and as decreases in dissolved sulfate downcore that vary in magnitude from site to site. Pore-water ammonium (NH_4^+) concentrations are strongly linked to release associated with decomposition of organic nitrogen compounds (Table 1). Nevertheless, mass balance considerations based on the reaction stoichiometry for bacterial sulfate reduction (assuming a Redfield C:N ratio), as well as the observed downcore variability in concentration, suggest that uptake of biologically liberated ammonium during silicate alteration (ion exchange reactions) is likely a factor (Berner, 1980). Downcore and intersite relationships for dissolved phosphate, although being sourced by organic decomposition, are complicated by the effective adsorption of phosphate onto the surfaces of carbonate sediment (Walter and Burton, 1986; Morse and Mackenzie, 1990).

Increases in pore-water manganese and iron record microbially mediated reductive dissolution of manganese and iron oxides and oxyhydroxides, whereas sinks are represented by incorporation into calcite (Dromgoole and Walter, 1990; Morse and Mackenzie, 1990) and by iron sulfide formation (Berner, 1984), albeit of generally minor extent for the latter. Downcore variability in the dissolved iron and manganese reflects nonsteady-state concentrations of TOC and the reactive solid phases of iron and manganese. These concentration relationships are linked in part to variations in calcium carbonate accumulation (i.e., varying dilution effects). Differences also reflect variation in the provenance of the solid manganese and iron as recorded in varying Mn/Ti and Fe/Ti ratios in the host sediments. Alkalinity (bicarbonate) levels are strongly influenced by production during organic decomposition (i.e., oxidation of organic matter), although carbonate reactions overprint the redox pathways (Table 1). Details of redox relationships are well represented in the data from Site 999 (Fig. 2) and in site chapters provided in Sigurdsson, Leckie, Acton, et al. (1997). Aspects of sulfate reduction will, however, be explored in further detail.

Generally low levels of sulfate reduction are corroborated by the paucity of methane in the headspace gases collected at the four sites (see exception at Site 1000 discussed below under the "Carbonate Reactions" section). The observed deficiencies in methane are expected given that appreciable methanogenesis occurs only after sulfate is depleted and sulfate reduction gives way to methane generation in the hierarchy of bacterial redox reactions observed in marine sediments (Martens and Berner, 1974; Froelich et al., 1979; Berner, 1980). To compare rates of sulfate reduction among Leg 165 sites and

Table 1. Representative reactions.

Carbonate reactions
Calcite/aragonite dissolution/precipitation:
$H_2O + CO_2 + CaCO_3 = Ca^{2+} + 2HCO_3^-$
Dolomite dissolution/precipitation:
$2H_2O + 2CO_2 + CaMg(CO_3)_2 = Ca^{2+} + Mg^{2+} + 4HCO_3^-$
Organic remineralization (redox pathways)
Suboxic diagenesis:
Mn and Fe reduction → dissolved Mn^{2+} and Fe^{2+} increase
Sulfate reduction:
$(CH_2O)_{106}(NH_3)_{16}(H_3PO_4) + 53SO_4^{2-} \rightarrow 106HCO_3^- + 53HS^- + 16NH_3 + H_3PO_4 + 53H^+$
Silicate reactions
Low-temperature decomposition (dissolution/hydrolysis) of basaltic basement:
basaltic glass, plagioclase, and olivine → e.g., release of Ca^{2+}, Mg^{2+}, Fe^{2+}, HCO_3^-, and H_4SiO_4
(liberated Mg^{2+}, H_4SiO_4, and Fe^{2+} rapidly removed via smectite precipitation)
K-feldspar → kaolinite:
$2KAlSi_3O_8 + 2H^+ + 9H_2O \rightarrow Al_2Si_2O_5(OH)_4 + 2K^+ + 4H_4SiO_4$
Kaolinite → illite:
$5Al_2Si_2O_5(OH)_4 + 2K^+ + 2HCO_3^- + 4SiO_{2(aq)} \rightarrow 2KAl_5Si_7O_{20}(OH)_4 + 7H_2O + 2CO_2$
Kaolinite → Mg-smectite:
$7Al_2Si_2O_5(OH)_4 + 8SiO_{2(aq)} + Mg^{2+} \rightarrow 6[(Al_{2.00})(Si_{3.67}Al_{0.33})O_{10}(OH)_2]Mg_{0.167} + 7H_2O + 2H^+$
Albite → Na-smectite:
$2.33NaAlSi_3O_8 + 8.64H_2O + 2CO_2 \rightarrow Na_{0.33}Al_{2.33}Si_{3.67}O_{10}(OH)_2 + 2Na^+ + 2HCO_3^- + 3.32H_4SiO_4$

relative to deep-sea sediments throughout the world, depth-integrated rates (mmol SO_4^{2-} cm^{-2} yr^{-1}) were modeled at Sites 998, 999, 1000, 1001 (Berner, 1980; Canfield, 1991):

$$\text{Rate} = \phi D_s dC/dx + \phi_o \omega C_o - \phi_b \omega C_b,$$

where ø is the average porosity in the zone (depth interval) of sulfate reduction, and dC is taken as the overall change in sulfate concentration over the zone of sulfate reduction (dx). This approach simplifies the expression by assuming a linear decrease in sulfate concentration over the interval of interest, which yields approximate and minimum estimates that are sufficient for our general comparative purposes given the shapes of the observed profiles. C_o and C_b are the concentrations of sulfate at the sediment/water interface (assumed to be the seawater value of 28.9 mM) and at the base of the zone of sulfate reduction, respectively. Porosity at the sediment/water interface and at the base of the zone of sulfate reduction are represented by ϕ_o and ϕ_b, respectively. D_s is the diffusion coefficient for dissolved sulfate in sediment, which is affected by temperature and the tortuosity of the sediment (Li and Gregory, 1974; Berner, 1980). Ultimately, the value for D_s was carefully chosen (Table 2) based on a recent evaluation of the effects of sediment type and porosity/tortuosity (Iversen and Jørgensen, 1993). The assumption of a constant D_s value within the zone of sulfate reduction is a simplification, given variations in porosity as a function of depth, but is warranted in light of the objectives of the study and the comparatively minor impact a more rigorous approach would have on the conclusions. The average sedimentation rate over the zone of sulfate reduction is indicated as ω.

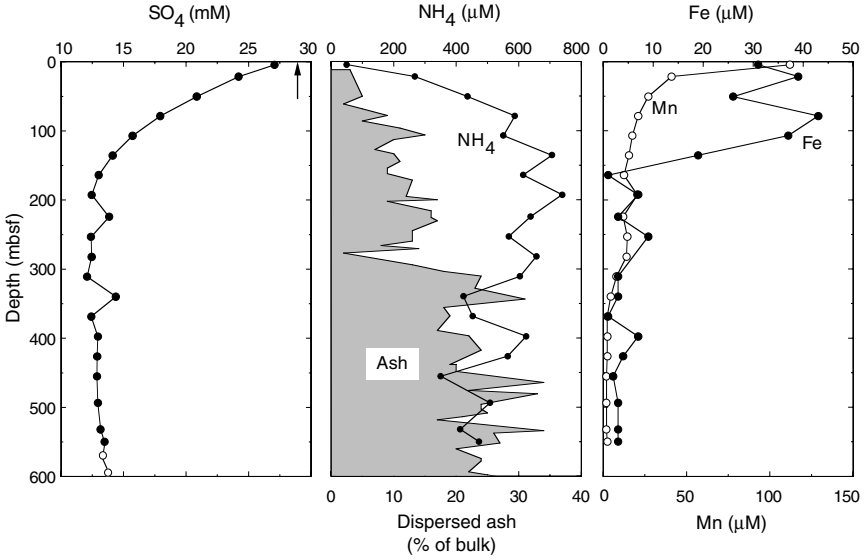

Figure 2. Depth profiles for sulfate, ammonium, manganese (open circles), and iron (solid circles) in Site 999 interstitial waters. The fraction of bulk sediment composed of dispersed volcanic ash (shaded area) is plotted vs. depth on the ammonium profile to permit evaluation of the effect of ash alteration on pore-water ammonium concentrations. The arrow indicates mean ocean bottom-water sulfate concentration. The two symbols (open and solid) used in the sulfate profile reflect the incorporation of data from two holes at Site 999.

Table 2. Modeled sulfate reduction rates.

	Site 998	Site 999	Site 1000	Site 1001
Depth to asymptotic SO_4^{2-} concentration (mbsf):	Not achieved; "linear" decrease to deepest sample (515.5 mbsf)	192.6	384.6	Not achieved; "linear" decrease to deepest sample (365.4 mbsf)
dC (in mM relative to 28.9 mM of overlying seawater):	(28.9-21.0)	(28.9-12.5)	(28.9-17.0)* (17.0-1.29)†	(28.9-23.5)** (23.5-18.9)‡
ϕ_o:	0.78	0.79	0.70* 0.60†	0.67** 0.60‡
ϕ_b:	0.51	0.60	0.60* 0.58†	0.63** 0.40‡
ø:	0.60	0.65	0.65* 0.59†	0.63** 0.44‡
ω (m/m.y.):	16.1	27.5	33.4* 33.4†	13.8** 16.7‡
D_s (cm^2 s^{-1}):	2.0×10^{-6}	2.0×10^{-6}	2.0×10^{-6}	2.0×10^{-6}
Depth-integrated sulfate reduction rate (mmol cm^{-2} yr^{-1}): Total:	2.5×10^{-5}	7.7×10^{-5}	$13.1 \times 10^{-5*}$ $4.9 \times 10^{-5\dagger}$ 18.0×10^{-5}	$1.9 \times 10^{-5**}$ $1.7 \times 10^{-5\ddagger}$ 3.6×10^{-5}
Mean total organic carbon (wt%):	0.007	0.13	0.15	0.03** 0.02‡
Mean total sulfur (wt%):	0.06	0.08	0.10	0.16** 0.05‡

Notes: For nonasymptotic sites (Sites 998 and 1001), depth-integrated rates reflect sulfate reduction only within the interval analyzed and are therefore minimum estimates. The asymptotic sulfate trend at Site 999 was treated as a single linear decrease. The asymptotic decrease at Site 1000 was divided into two distinct linear trends; each was treated separately in the calculations: * = depths of 0–50 mbsf, † = depths of 50–384.6 mbsf. Site 1001 is characterized by a major unconformity at ~165 mbsf. Intervals above and below were treated separately: ** = depths of 0–165 mbsf, ‡ = depths of 165–365.4 mbsf. Complete data are available in Sigurdsson, Leckie, Acton, et al. (1997). See text for equation and full explanation of parameters.

These estimated parameters (based on data in Sigurdsson, Leckie, Acton, et al., 1997) and the calculated depth-integrated sulfate reduction rates are summarized in Table 2. The calculations are predicated on the assumption that infaunal mixing is not a factor over the zone of interest, which is justified given depths of tens to hundreds of meters for the zones of sulfate decrease at these sites (Canfield, 1991). The base of the zone of sulfate reduction is typically delineated by the attainment of asymptotic sulfate concentrations (Sites 999 and 1000); however, such concentrations are not observed over the analyzed intervals at Sites 998 and 1001. Consequently, the calculation can only be performed over zones of steadily decreasing sulfate for these latter sites and thus yields minimum values for the total depth-integrated rate of sulfate reduction. Furthermore, given the presence of a temporally significant unconformity at Site 1001, the sampled intervals above and below the hiatus were treated separately in the calculation and summed for a total rate (Table 2).

To test the validity of treating the sulfate trends (dC/dx) as linear, the sulfate profile from Site 1000 was subdivided into two distinct linear trends to account for the "steeper" sulfate depletion in the upper 50 meters below seafloor (mbsf) (Table 2). Of the four sites, this profile is least effectively represented by a single linear approximation, yet the calculated depth-integrated sulfate reduction rates differ only by a factor of 1.9 for this most extreme example: 9.3×10^{-5} mmol cm^{-2} yr^{-1} vs. 18.0×10^{-5} mmol cm^{-2} yr^{-1} for approximation via one vs. two lines, respectively. The sulfate profile for Site 1000 is provided in the "Carbonate Reactions" section.

In a general sense, the calculated rates of sulfate reduction (in mmol cm^{-2} yr^{-1}), which range from 2.5×10^{-5} to 18.0×10^{-5} (Table 2), are low and consistent with the rates presented by Canfield (1991) for deep-sea sediments along the margins of ocean basins. This fundamental conclusion is insensitive to any reasonable manipulation of the calculation outlined above (e.g., choice of D_s or curve fitting the sulfate data). By contrast, the organic-rich surface sediments of the anoxic Cariaco Basin (Shipboard Scientific Party, 1997d) show a tenfold decrease in dissolved sulfate concentration over only 6 m of burial depth (see Lyons et al., 1998). Although the rates presented in Table 2 are only estimates, they do show a general positive relationship with respect to TOC concentration over the narrow ranges for both parameters. Sulfate depletion at Site 1000 is further complicated by the possibility of gaseous hydrocarbons providing additional electron donors to facilitate bacterial sulfate reduction. Details for Site 1000 are provided below in the "Carbonate Reactions" discussion.

The low TOC values and correspondingly low rates of sulfate reduction are ultimately a function of generally low surface primary production away from continental margins (coastal upwelling) and the great water depths and slow rates of sediment accumulation at the Leg 165 sites. Suess (1980) and others have demonstrated a strong inverse relationship between water depth and the percent of surface organic-carbon production preserved, reflecting progressive degradation within the settling particulates. Furthermore, it is well established that carbon burial efficiency (i.e., the proportion of the flux of organic carbon to the sediment surface that survives diagenetic oxidation and becomes permanently buried) is positively related to sedimentation rate (Müller and Suess, 1979; Henrichs and Reeburgh, 1987; Canfield, 1989b, 1994). Rapid burial not only fosters enhanced preservation but also increases the availability of reactive organic phases for sulfate reduction (i.e., favors enhanced survival from aerobic respiration in the uppermost layers). This relationship manifests as a positive correlation between the rate constant for sulfate reduction (k) and sedimentation rate (ω) (Toth and Lerman, 1977; Berner, 1978, 1980), which can be stated as

$$k = A\omega^2,$$

where A is an empirical constant. Consequently, the comparatively low rates of accumulation at the pelagic to hemipelagic sites of Leg 165 are consistent with both low rates of sulfate reduction and porewater profiles bearing strong signals of suboxic redox processes.

Given the low rates of sulfate reduction summarized in Table 2 and the aforementioned strength of the suboxic signal, it is not surprising to see low total sulfur contents in the sediments, with mean values of ≤0.16 wt% (Table 2). Despite the availability of iron, inadequate supplies of bacterially produced H_2S limit the amount of sedimentary pyrite formation. In other words, detritally delivered reactive iron is in sufficient supply despite the high dilution by calcium carbonate (Berner, 1984; Canfield, 1989a; Canfield et al., 1992; Lyons and Berner, 1992; Raiswell and Canfield, 1998). Overall, total sulfur concentrations, which reflect pyrite in these sediments, are generally low and nonsystematic in the sediments at the four sites (e.g., Fig. 3).

Notable exceptions to the low pyrite sulfur contents are several of the discrete volcanic ash layers within the cores where pyrite enrichments, as secondary overgrowths on ash fragments, were first observed on board and later substantiated via the chromium reduction method described above (Table 3). It should be noted that these "discrete" layers, in many cases, bear bioturbational overprints of varying degrees. In addition to elevated sulfur contents, the ashes also show trace-metal concentrations that are enriched, particularly for nickel, relative to the host sediments and expected concentrations given the lithologies of the ash layers (Table 3) (Sigurdsson, Leckie, Acton, et al., 1997). This relationship is particularly well expressed in the ash layers from Site 999 where there is a general correlation between nickel and sulfur contents (Fig. 4). Furthermore, Site 999 shows unusually nonsystematic variation in pyrite sulfur content within the routinely analyzed bulk sediment samples (Fig. 3). This distribution of sulfur is reminiscent of the downcore variability that characterizes the distribution of ash within the core.

Preliminary evaluations suggest that secondary nickel and sulfur enrichments may be linked mechanistically to externally derived fluids bearing sulfide and metals that follow permeability pathways con-

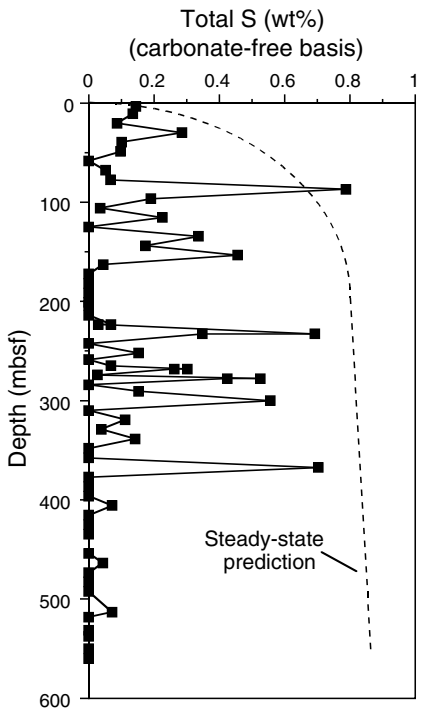

Figure 3. Downcore distribution of total sulfur concentrations at Site 999 reported as weight percent on a carbonate-free basis to remove dilution effects. The total sulfur values are thought to represent pyrite in these samples. A schematic representation of the predicted distribution of pyrite sulfur for a steady-state diagenetic system has been included for comparison. This idealized profile is not based on parameters of the actual host sediment, so the general shape rather than the absolute concentrations is the most meaningful aspect for comparison.

Table 3. Geochemical data for discrete ash* layers.

Core, section, interval (cm)	S† (wt%)	$\delta^{34}S$ (‰)‡	Ni (ppm)**
165-998A-			
13H-3, 25-27	0.01	††	187
13H-5, 118-120	0.02	††	90
14H-6, 16-18	0.03	††	134
20X-2, 9-11	0.01	††	9
20X-CC, 32-33	0.01	††	9
37X-1, 142-144	0.03	††	173
165-998B-			
1R-7, 51-53	1.91(?)‡‡	††	84
9R-4, 48-50	0.02	††	115
31R-CC, 5-7	0.01	††	97
33R-2, 88-91	0.02	††	††
35R-5, 109-111	0.33	††	319
35R-6, 68-71	0.18	††	25
165-999A-			
17H-4, 112-114	1.72	††	514
20H-2, 142-144	1.24	-30.9***	233
28X-5, 15-18	0.61	-34.9	223
32X-1, 107-109	2.26	-32.9	554
34X-3, 51-54	0.80	-29.2	239
37X-6, 98-100	0.51	-35.4	61
39X-2, 8-11	0.37	-34.6	56
42X-1, 68-70	0.07	††	26
45X-5, 123-125	0.27	-41.4 †††	83
46X-2, 11-13	0.06	††	90
48X-1, 14-16	1.68	††	††
58X-5, 57-60	0.03	††	††
165-999B-			
9R-2, 98-102	0.08	††	26
24R-3, 103-107	0.10	††	57
38R-2, 135-137	0.02	††	††
165-1000B-			
6R-4, 143-145	0.70	-26.9	153
11R-1, 142-145	0.06	††	6
21R-4, 43-46	0.21	-27.1	3
165-1001B-			
31R-5, 37-39	0.03	††	74

Notes: * = see text for relevant caveats. † = total Cr-reducible S; see text for details. ‡ = total Cr-reducible S; relative to CDT standard. ** = complete trace element data and analytical details are available in Sigurdsson, Leckie, Acton, et al. (1997). †† = data not available; missing $\delta^{34}S$ data reflect small ash samples and/or low S content. ‡‡ = very low Ag_2S yield during Cr-reduction for $\delta^{34}S$ determination. *** = small sample; acceptable gas yield. ††† = small SO_2 yield.

trolled by ash distribution. It is important to note that the pyrite enrichments do not reflect local sites of enhanced sulfate reduction (i.e., organic enrichment) or iron availability (iron is not limiting throughout the host sediments). Thus, it is difficult to envision the establishment of concentration gradients toward the ash layers. It is also important to note that this phenomenon is best expressed at Site 999 where high-angle faulting has been described in detail (Shipboard Scientific Party, 1997a). The sulfur isotope data—with the striking presence of ^{34}S-depleted values—are unambiguous in delineating a bacterial source for the sulfide (Ohmoto, 1972; Chambers and Trudinger, 1979; Machel et al., 1995; Lyons, 1997; Raiswell, 1997), which precludes basement-derived magmatic fluids or thermochemical sulfate reduction as a source for the sulfur (Table 3). The suggestion, therefore, is that bacterial sulfate reduction is occurring away from the sites of mineralization, perhaps deep within the sediment package, and that reducing fluids may be moving up along fault conduits and mineralizing the ash layers and, to a lesser extent, the adjacent host sediments. Such a model could also explain the atypical sulfur distribution in Figure 3. At this juncture we cannot preclude a basement origin for the metals, and the mechanistic details of metal and sulfur transport and emplacement, including the timing, remain uncertain.

CARBONATE REACTIONS

The sediments at Sites 998, 999, 1000, and 1001 are characterized by high concentrations of calcium carbonate, with mean values of

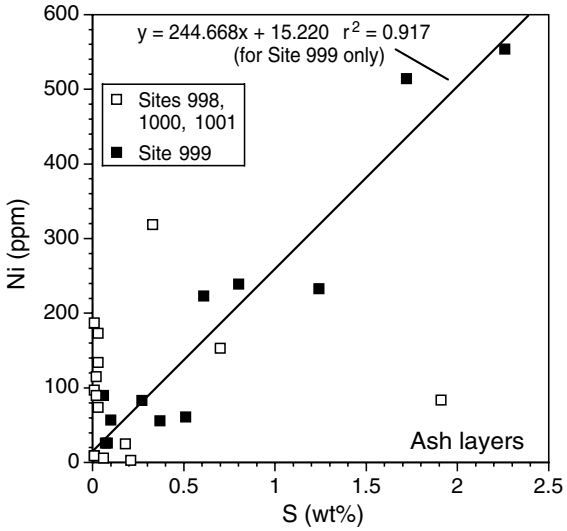

Figure 4. Plot of Cr-reducible sulfur vs. total Ni in discrete volcanic ash layers from Sites 998, 999, 1000, and 1001 (see Table 3 for data). Cr-reducible sulfur is thought to represent pyrite in these samples. A linear regression fit has been included for Site 999 (solid squares) only.

77.9, 58.6, 80.6, and 68.1 wt%, respectively. Consequently, the pore-water profiles for a range of species, including calcium, magnesium, strontium, and alkalinity (bicarbonate), are intimately linked to dissolution and precipitation of reactive carbonate phases (e.g., Emerson et al., 1980; Archer et al., 1989; Morse and Mackenzie, 1990). This is particularly well expressed at Site 1000 (Fig. 5), where aragonite dissolution and/or inversion to calcite and deep precipitation of calcium carbonate (for reasons outlined below) appear to be dominant factors. Although not simple relationships, these reactions are reflected at Site 1000 by the general correspondence between dissolved calcium and strontium (Sr is enriched in aragonite); however, the decrease in dissolved strontium deeper in the core is less well understood and may reflect deep precipitation of aragonite or, more likely, celestite precipitation or adsorption onto clay minerals (Shipboard Scientific Party, 1997b). Precipitation of celestite ($SrSO_4$) is consistent with the high levels of dissolved strontium observed at Site 1000 (Fig. 5) and would contribute to the observed downcore decrease in dissolved sulfate; however, the strontium concentration continues to drop at depths below the attainment of asymptotic pore-water sulfate concentrations. The sulfate profile is provided later in this discussion.

What is perhaps most striking at Site 1000 and most consistent with carbonate reactions occurring within the sediment is the observed relationship between dissolved calcium and magnesium (Fig. 5). Well-developed downcore increases in dissolved calcium and corresponding systematic decreases in magnesium are a common observation in pelagic sediments (Gieskes, 1981, 1983). The lack of this simple inverse relationship at Site 1000 (Fig. 6) has important implications. Simply put, inverse behavior has been linked in past studies to calcium carbonate dissolution, dissolution of volcanic glass, and carbonate and silicate reactions within the sediments (Table 1), including the formation of Mg-rich smectite and dolomite. However, the best defined inverse relationships are often attributed to low-temperature alteration of basement basalt, whereby the observed pore-water profiles dominantly reflect diffusion between the overlying seawater and the underlying basaltic crust.

Extensive effort has been made to distinguish among the various internal (i.e., within the sediments) and external sources and sinks for dissolved calcium and magnesium. For example, McDuff and Gieskes (1976) and McDuff (1981) argued that a comparison between measured values and modeled diffusion profiles would yield an indication of conservative behavior (i.e., extent of reaction within the sediment column) for both calcium and magnesium (see also Ler-

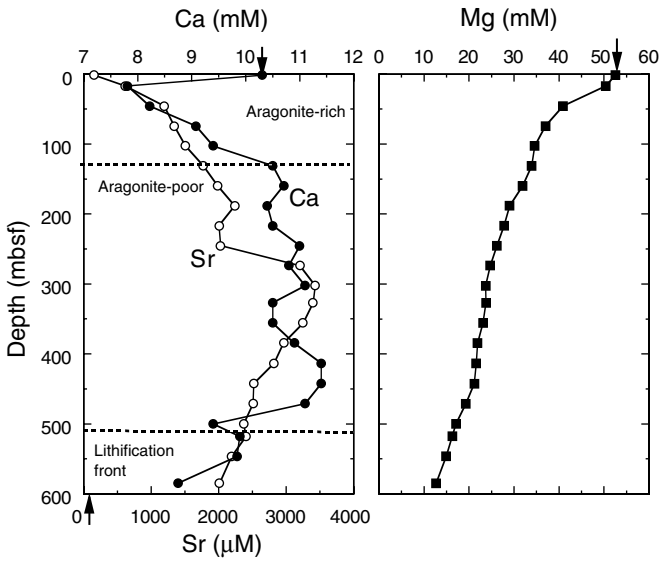

Figure 5. Depth profile for calcium (solid circles), strontium (open circles), and magnesium in Site 1000 interstitial waters. The arrows indicate mean ocean bottom-water concentrations for each of the three species.

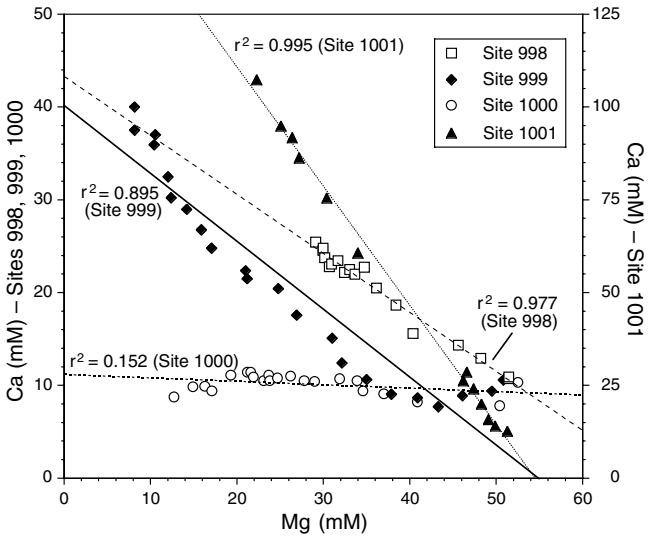

Figure 6. Plot of pore-water magnesium vs. calcium for Sites 998, 999, 1000, and 1001. Linear regression fits have been included for the data from each of the four sites.

man, 1975; Kastner and Gieskes, 1976; Gieskes, 1983). Differences in the two profiles can be ascribed to the carbonate and silicate reactions addressed in Table 1 and approximated by deviance from a simple inverse linear relationship between concentrations of dissolved calcium and magnesium (Fig. 6). Clearly, Figures 5 and 6 show that a simple inverse relationship between the two species is not observed at Site 1000, suggesting nonconservative behavior linked at least in part to carbonate diagenesis. Further details and the implications of this observation will be addressed in greater detail below in the "Basaltic Basement/Seawater Reactions" section.

The suggestion that deep calcium carbonate precipitation may be occurring at Site 1000 is well supported by a range of independent observations, including a downcore decrease in alkalinity (Fig. 7; Table 1). This site is unique in a number of respects: (1) there is an abrupt downcore transition between poorly lithified and well-lithified limestone (Fig. 7); (2) there is an interval of pronounced subsurface enrichment in volatile hydrocarbons bounded by the minimum in solid-phase calcium carbonate and the "lithification front" marking the transition into well-lithified limestone (Figs. 7, 8); (3) there is a downcore increase in TOC content (Fig. 9); and (4) the near zero asymptotic concentration of sulfate corresponds very closely with the top of the carbonate minimum zone (Miocene carbonate "crash") and the top of the hydrocarbon-enriched interval (Fig. 10). Details are provided by the Shipboard Scientific Party (1997b), including extensive discussion addressing the character and origin of the middle/late Miocene carbonate concentration/accumulation "crash," but are summarized as follows.

The enrichment in volatile hydrocarbons is thought to represent trapping of thermogenic gases below a permeability seal caused by the reduction in carbonate content. The external origin of these gases is supported by present burial depths and maximum temperature estimates based on Rock-Eval pyrolysis that argue against sufficient thermal maturation of the local organic matter (Shipboard Scientific Party, 1997b). The enrichments in hydrocarbons (dominated by methane; Fig. 8) and the greater TOC values in this portion of the core may drive enhanced rates of microbial reaction, including sulfate reduction (see Shaw and Meyers, 1996, for a discussion on methane as a carbon source for sulfate reduction). In other words, cementation defining the lithification front could be driven by bicarbonate production resulting from the oxidation of both solid and gaseous

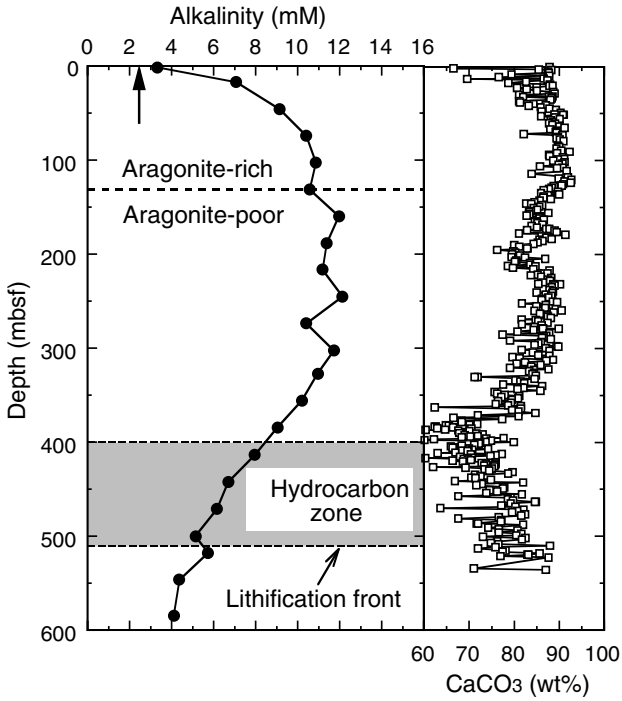

Figure 7. Depth profile for total alkalinity in Site 1000 interstitial waters. Bulk sediment calcium carbonate contents are also included. The "hydrocarbon zone" is defined in the text and subsequent figures. The arrow indicates mean ocean bottom-water alkalinity.

carbon compounds (Table 1). The low sulfate concentrations in the hydrocarbon zone (Fig. 10) suggest that in situ methanogenesis may be a factor; however, the broader array of hydrocarbons in the zone (C_2 and greater; Fig. 8) eliminate bacterial production as the only gas source.

The position of the cementation front may be controlled by equilibrium relationships (i.e., saturation states) or kinetic (nucleation) considerations whereby precipitation is favored by the more carbon-

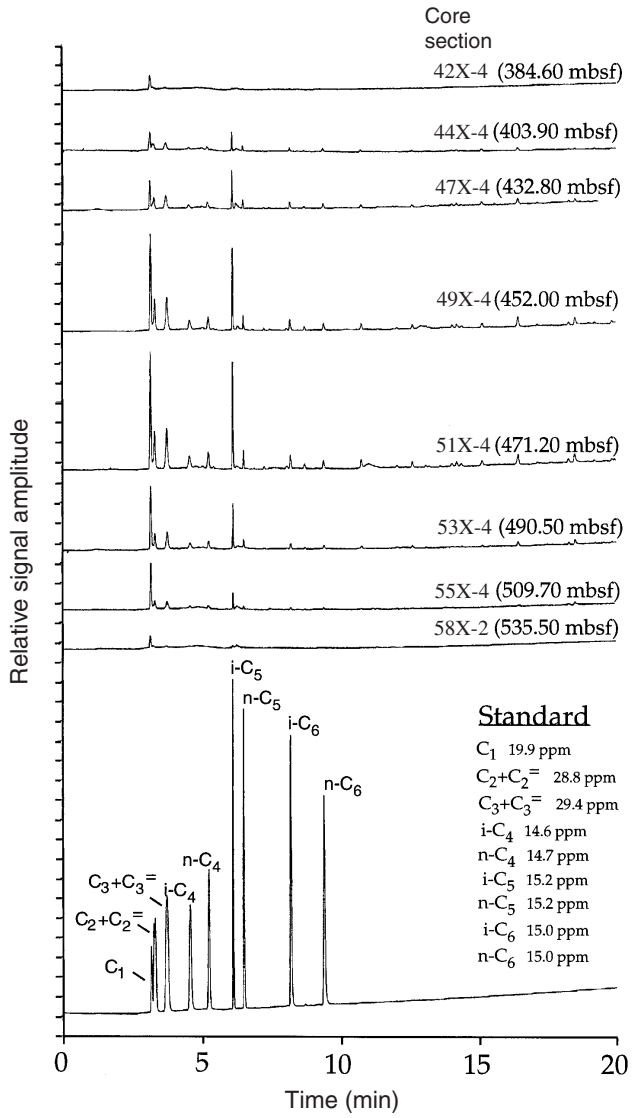

Figure 8. Chromatogram composite from the zone of volatile hydrocarbon enrichment at Site 1000 (see text and related figures). Data from overlying and underlying hydrocarbon-deficient zones are included for comparison. Concentrations can be estimated by comparing signal amplitudes (peak heights) of the sample intervals to those of the standard. Vertical scales are constant, and a linear correspondence between the unknowns and the standard can be assumed for a given hydrocarbon.

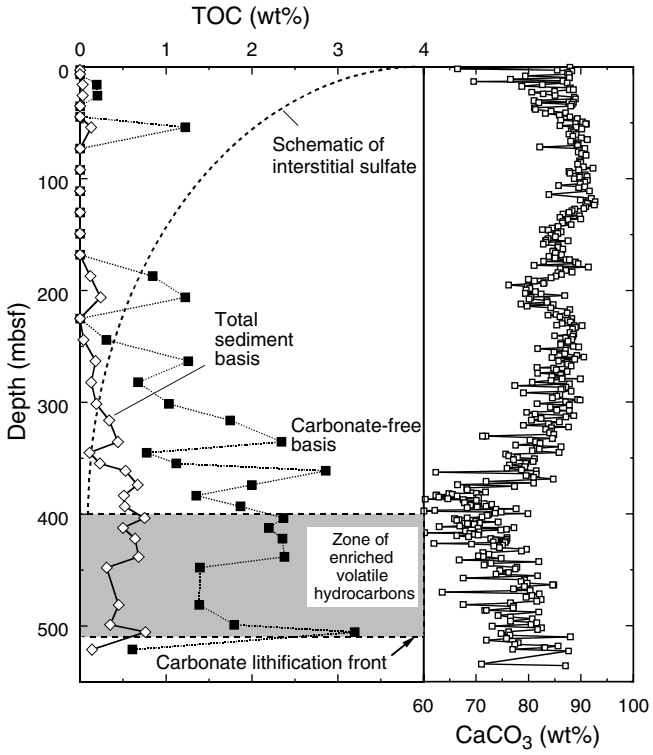

Figure 9. Depth profile for total organic carbon (TOC) for Site 1000 reported as weight percent on a total sediment basis (open diamonds) and a carbonate-free basis (solid squares). A schematic of the interstitial sulfate profile has been included for comparison (see Fig. 10 for the actual profile). Concentrations of calcium carbonate over the same interval and the stratigraphic position of the hydrocarbon-enriched zone are also included (see text for discussion).

ate-rich substrate beneath the carbonate minimum. The associated cementation would give rise to the observed decreases in dissolved calcium and alkalinity, as well as strontium if aragonite is precipitated (Figs. 5, 7; Table 1). This model, invoking deep-burial microbial mediation, is speculative and not supported by preliminary $\delta^{13}C$ measurements of the well-cemented limestones (M. Mutti, pers. comm., 1998); however, the isotopic data may be dominated by substrate compositions (i.e., host sediments rather than the inferred "late-stage" cement). Furthermore, the striking stratigraphic correspondence among a diverse range of geochemical parameters is undeniable. It should also be noted that the upward curvature of the sulfate profile and the model results of Table 2 indicate that sulfate reduction is occurring throughout the sediment column, including maximum calculated rates in the upper 50 mbsf. In a more general sense, enhanced carbonate reactivity at Site 1000, in terms of both deep precipitation and aragonite dissolution in the upper layers, agrees with the absence of a linear inverse relationship in Figures 5 and 6, where the downcore decrease in dissolved magnesium may reflect deeper reactions with basaltic crust, but the expected corresponding increase in calcium is buffered by precipitation reactions within the sediment column.

BASALTIC BASEMENT/SEAWATER REACTIONS

In contrast to the complexities at Site 1000, the remaining three sites show significantly more robust inverse relationships between calcium and magnesium in the pore waters (Fig. 6), suggesting strong controls linked to alteration of basaltic basement and arguing for sediment pore-water profiles that correspondingly reflect diffusion between the overlying seawater and underlying basaltic crust. This relationship is best expressed in the striking mirror-image profiles for dissolved calcium and magnesium at Site 1001 (Fig. 11). The calcium and magnesium profiles for Site 999 (not shown; see Shipboard Scientific Party, 1997a) and the weaker linear relationship in Figure 6 suggest that sediment reactions may play a more significant role, although nonconservative behavior is undoubtedly a factor at all three sites (see "Alteration of Volcanic Ash" section, below). For example, despite the strong inverse relationship and the mirror-image profiles between calcium and magnesium displayed in Figures 6 and 12, respectively, the upward curvature of the Site 998 profiles suggests that much of the calcium and magnesium variation may be because of reactions in the sediment. Concentrations of dissolved strontium at Sites 998, 999, and 1001 (see Figs. 11, 12) (Shipboard Scientific Par-

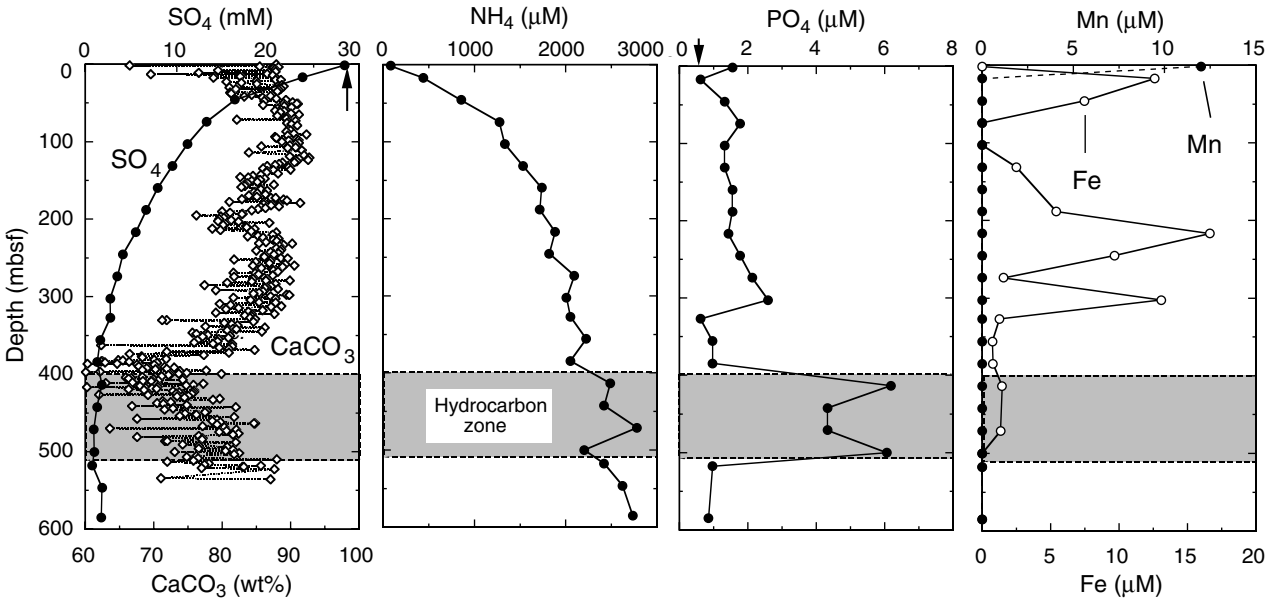

Figure 10. Depth profiles for sulfate, ammonium, phosphate, manganese, and iron in Site 1000 interstitial waters. Bulk sediment calcium carbonate contents are also included. The "hydrocarbon zone" is defined in the text and related figures. The arrow indicates mean ocean bottom-water sulfate concentration.

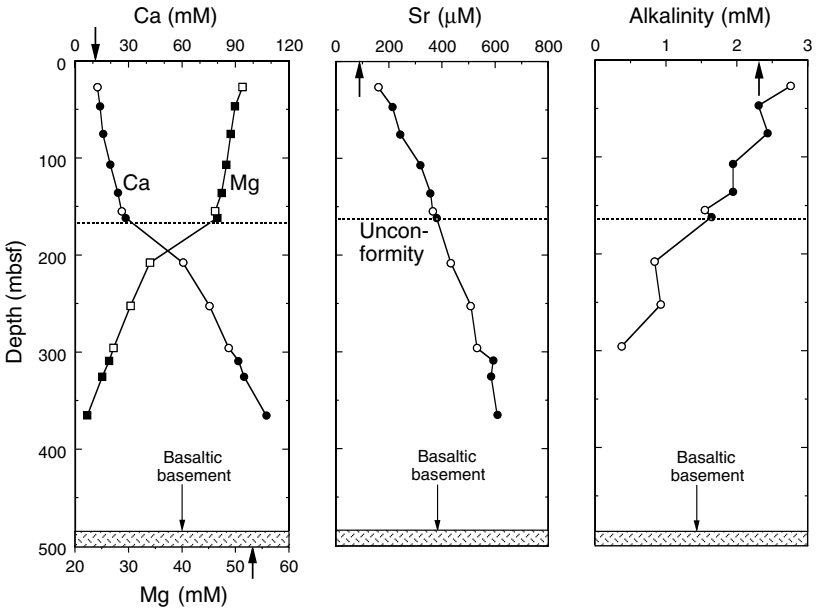

Figure 11. Depth profiles for calcium (open and solid circles) and magnesium (open and solid squares), strontium, and total alkalinity in Site 1001 interstitial waters. The stratigraphic position of a major unconformity (see text and Sigurdsson, Leckie, Acton, et al., 1997, for details) and the basaltic basement are indicated. The arrows indicate mean ocean bottom-water concentrations for each of the four species. The two symbols (open and solid) used in the calcium and magnesium profiles reflect the incorporation of data from two holes at Site 1001.

ty, 1997a) appear to be controlled by a combination of carbonate reactions, alteration of basaltic basement, and likely reactions involving interbedded and dispersed volcanic ash, although $^{87}Sr/^{86}Sr$ relationships are required to resolve the relative contributions (Gieskes, 1981, 1983; Gieskes et al., 1998).

In terms of low-temperature interactions between seawater and basaltic basement (see Gieskes, 1981, 1983; Thompson, 1983; Berner and Berner, 1996), the critical reactions include the decomposition (hydrolysis/dissolution) of basaltic glass, calcic plagioclase, and olivine—which liberate Ca^{2+}, Mg^{2+}, Fe^{2+}, bicarbonate, and silica—and the rapid precipitation of smectite that serves as an essential sink for Mg^{2+} (e.g., Seyfried and Bischoff, 1981; Staudigel and Hart, 1983) (Table 1). It is also certain that the formation of additional silicate phases (clay minerals and zeolites) in association with basalt alteration acts as an important sink (and source) for a wide range of cations. The downcore increase in calcium is the most striking pore-water manifestation of basalt alteration at Site 1001 (Fig. 11), with increases greater than those at Sites 998 and 999 by factors of ~4 and 2.5, respectively. This relationship attests to the strong basement alteration signal in the pore waters at Site 1001 (Fig. 6). The corresponding decrease in alkalinity is thought to reflect the precipitation of calcium carbonate as abundant calcite veins present throughout the altered basalt (Table 1), although mass-balance confirmation was not attempted, and the associated Ca^{2+} sink is overwhelmed by the basalt source term. General styles of basalt alteration at Site 1001, including the precipitated vein calcite, are documented in Shipboard Scientific Party (1997c).

ALTERATION OF VOLCANIC ASH

Like the alteration of basaltic basement, patterns of silicate reaction within the sediments, or more specifically alteration of the abundant ash, influence the pore-water profiles at Sites 998, 999, 1000,

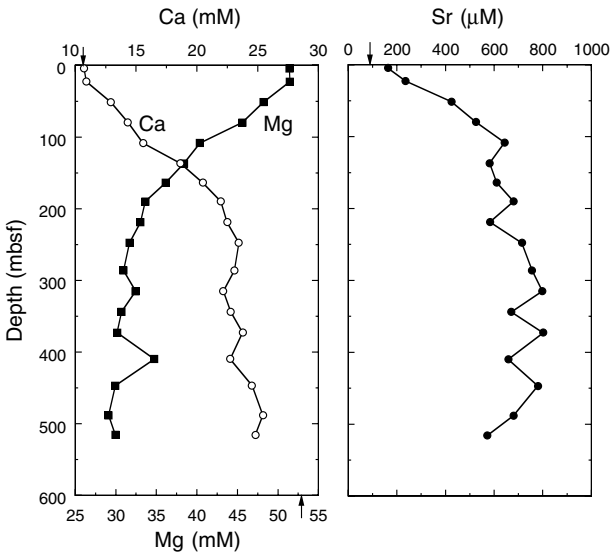

Figure 12. Depth profiles for calcium (open circles), magnesium (solid squares), and strontium in Site 998 interstitial waters. The arrows indicate mean ocean bottom-water concentrations for each of the three species.

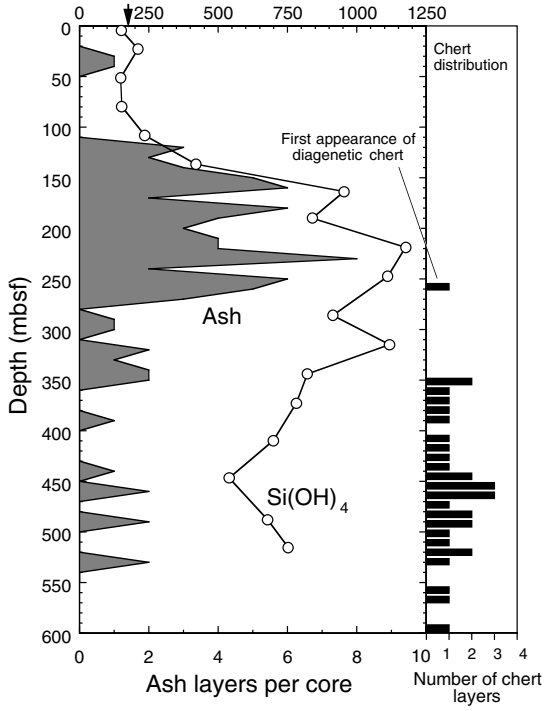

Figure 13. Depth profile for silica in Site 998 interstitial waters. Frequency of chert layers with depth are indicated in the histogram. Distribution of discrete ash layers (shaded area) is also included. The arrow indicates mean ocean bottom-water silica concentration.

and 1001 (Sigurdsson, Leckie, Acton, et al., 1997; see also Gieskes and Lawrence, 1981). The large volumes and frequencies of Eocene and Miocene silicic ash observed and quantified during Leg 165, both as discrete layers and fine disseminations within the host sediment, show undeniable stratigraphic correlations between their independently determined distributions and a wide range of dissolved species. For example, interstitial silica faithfully mirrors the ash distribution at Site 998 (Fig. 13), reflecting the release of silica during glass

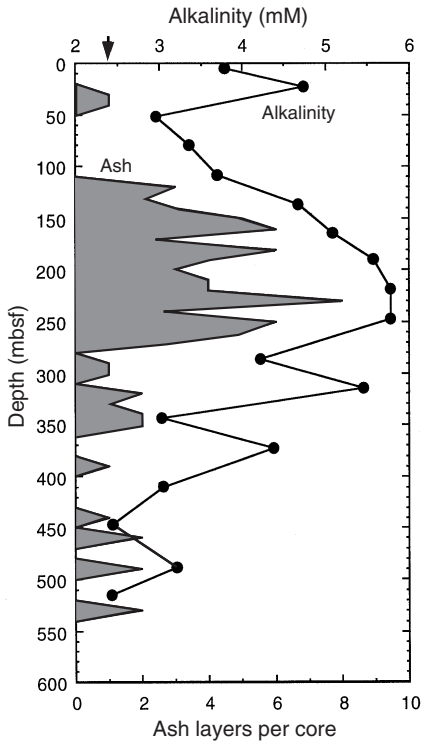

Figure 14. Depth profile for total alkalinity in Site 998 interstitial waters. Distribution of discrete ash layers (shaded area) is also included. The arrow indicates mean ocean bottom-water alkalinity.

dissolution/alteration and silicate hydrolysis during alteration of the ash (Table 1). Figure 13 also documents the correspondence between ash-related silica concentration and chert distribution, which acts as a sink for the dissolved silica. Furthermore, the silicate reactions (hydrolysis; e.g., Table 1) result in alkalinity relationships that are also strongly linked to ash distribution (e.g., Fig. 14). The fine ash disseminations within the host sediment were quantified using elemental mass balances (see Sigurdsson, Leckie, Acton, et al., 1997).

A similar relationship among volcanic ash, chert, and the concentration of silica is observed at Site 1001 (Fig. 15). Although chert formation may be possible at the stratigraphic level of first appearance (~165 mbsf), pre-unconformity physical conditions (specifically higher temperatures and greater burial depths) would have favored diagenetic precipitation. Consequently, we support pre-erosional chert formation with substantial removal of overlying sediment. This is substantiated by the almost 40 Ma represented by the hiatus between the Paleogene and Neogene sections in unconformable contact at ~165 mbsf (Shipboard Scientific Party, 1997c). Of interest, the ash-related pore-water enrichment in silica that is likely responsible for chert formation is still recorded at Site 1001 (Fig. 15), which suggests that ash alteration in this core, as in the others, is ongoing. Under the conditions of slow sediment accumulation of the present study (i.e., pelagic to hemipelagic rates), diffusion is sufficiently rapid to smooth out records of nonsteady-state sinks and sources of interstitial components unless the reactions are ongoing or occurred in the recent past (Lasaga and Holland, 1976).

The silica/ash relationship is also well recorded at Site 999 (Fig. 16), where a striking correspondence is observed among ash and dissolved silica distributions and the occurrence of biogenic silica. This important relationship likely represents the enhanced preservation of biogenic opaline silica within ash-rich intervals as a consequence of silica buffering during ash alteration (e.g., smectite formation; Table 1). Furthermore, the observed enhanced preservation of carbonate microfossils proximal to ash layers attests to the buffering capacity of alkalinity production associated with ash alteration (e.g., smectite

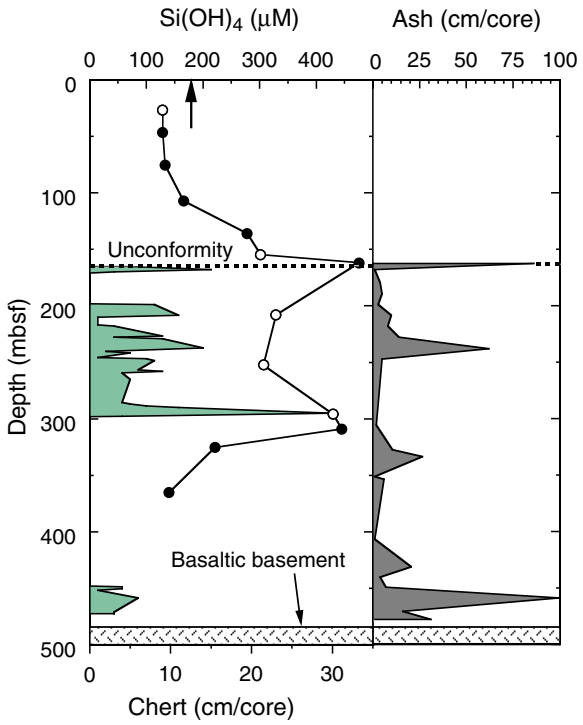

Figure 15. Depth profile for silica in Site 1001 interstitial waters. The stratigraphic position of a major unconformity (see text and Sigurdsson, Leckie, Acton, et al., 1997, for details) and the basaltic basement are indicated. Ash (as discrete layers) and chert distributions are also included. The arrow indicates mean ocean bottom-water silica concentration. The two symbols (open and solid) used in the silica profile reflect the incorporation of data from two holes at Site 1001.

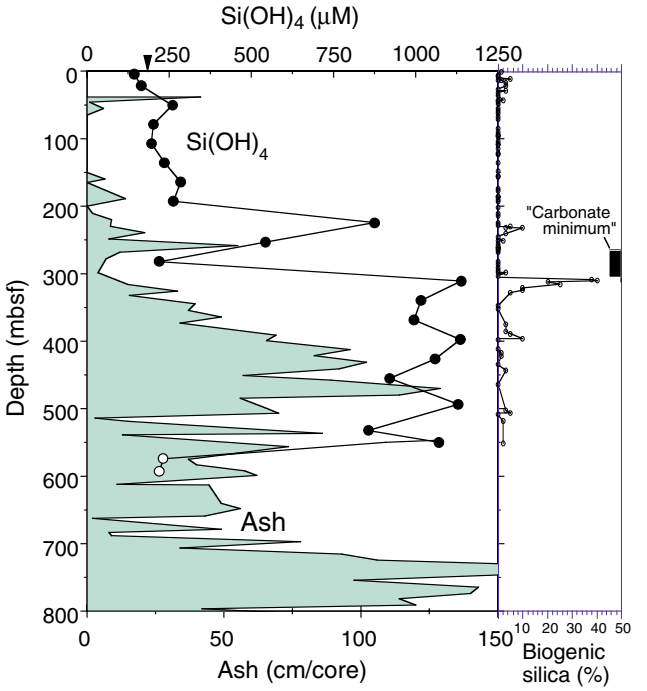

Figure 16. Depth profile for silica in Site 999 interstitial waters. Distribution of discrete ash layers (shaded area) is also included. Also plotted is the distribution of biogenic silica as determined by smear-slide analysis. The arrow indicates mean ocean bottom-water silica concentration. The two symbols (open and solid) used in the silica profile reflect the incorporation of data from two holes at Site 999.

formation). These observations have important taphonomic implications. Future studies should attempt to quantify the alteration of Eocene ashes—which are now known to represent a significant fraction of the Cenozoic stratigraphic section in the Caribbean—in its role toward imprinting levels of oceanic silica and ultimately catalyzing the accumulation of the vast amount of chert that abounds in the Eocene marine record (McGowran, 1989).

Important reactions between the volcanic ash and seawater include the dissolution/alteration (hydrolysis) of volcanic glasses and crystalline phases and the back precipitation (reverse weathering) that results in zeolites and clay minerals, including smectites (Table 1). These reactions, as sources and sinks, exert a strong control on the downcore distributions of a wide range of dissolved species, including cations such as rubidium, potassium, and lithium (see Sigurdsson, Leckie, Acton, et al., 1997, for extensive details). As an example, Figure 17 shows the downcore distribution of rubidium at Site 999 relative to both discrete ash layers and dispersed ash as quantified using independent elemental mass balances. This example is included to highlight the importance of not only the individual ash "events" but also the volumetric significance of the abundant reactive ash disseminated within the host sediments, reflecting perhaps a steady background flux of ash between major eruptions and/or the effects of bioturbational mixing that may be capable of obliterating the record of smaller events.

SUMMARY

These highlights from ODP Leg 165 emphasize the value in addressing the aqueous geochemical aspects of deep-marine sediments within a well-constrained, integrated context. By defining the system carefully in terms of both solid and dissolved species of varying concentrations and reactivities, the downcore distributions of a wide range of interstitial components are qualitatively and perhaps at least semiquantitatively interpretable with regard to rates and styles of sequestration and release. The above results, although only highlights, document the complex interplay among reactive carbonate phases, alteration of volcanic ash occurring as discrete layers and as a dispersed fraction within the host sediment, and alteration of the crystalline basement. Biogeochemical processes overprint many of the constituents as a function of the reactivity and availability of solid organic phases and, possibly, secondary hydrocarbon enrichments controlled by the physical properties of the sediment. In general, the sediments at Sites 998, 999, 1000, and 1001 are characterized by low levels of organic carbon and, correspondingly, microbial redox pathways dominated by suboxic process and low modeled levels of sulfate reduction. However, concentration and isotope relationships for sulfur, when viewed in conjunction with trace metal distributions, suggest that basinal fluids may epigenetically overprint permeable ash layers and associated sediments in tectonically active deep-sea settings such as Site 999. Finally, a better mechanistic understanding of these diverse processes further constrains the global mass balances for a wide range of major and minor components of seawater.

ACKNOWLEDGMENTS

The authors acknowledge with gratitude the many ODP staff members, both shipboard and shore-based, that facilitated the successful completion of this cruise. In particular, lab specialists D. Graham and J. Lee are thanked for their exhaustive efforts in generating high quality data. H. Sigurdsson, M. Leckie, and G. Acton are ac-

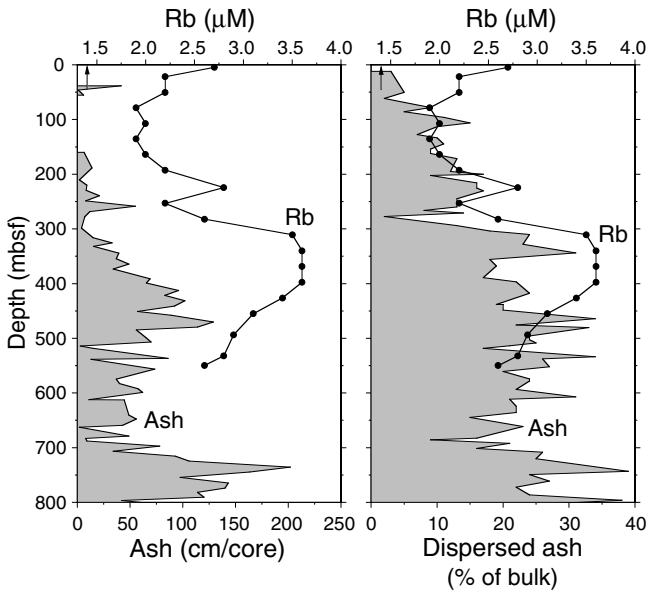

Figure 17. Depth profiles for rubidium in Site 999 interstitial waters. Distributions of both discrete ash layers and dispersed ash are included for comparison. The arrow indicates mean ocean bottom-water rubidium concentration.

knowledged for their yeoman's effort before, during, and after the cruise, as are the Sedco officials and crew members. B. Thomas, J. Luepke, K. Keel, and E. Grabowski are thanked for their work in the MU labs. K. Shelton provided access to the MU stable isotope facility. Partial financial support for this work and a postcruise geochemical study of Site 1002 was provided by JOI-USSSP. The manuscript benefited from reviews by J. Gieskes and P. Swart.

REFERENCES

Archer, D., Emerson, S., and Reimers, C., 1989. Dissolution of calcite in deep-sea sediments: pH and O_2 microelectrode results. *Geochim. Cosmochim. Acta,* 53:2831–2845.

Berner, E.K., and Berner, R.A., 1996. *Global Environment: Water, Air, and Geochemical Cycles*: Upper Saddle River, NJ (Prentice Hall).

Berner, R.A., 1978. Sulfate reduction and the rate of deposition of marine sediments. *Earth Planet. Sci. Lett.,* 37:492–498.

————, 1980. *Early Diagenesis: A Theoretical Approach:* Princeton, NJ (Princeton Univ. Press).

————, 1984. Sedimentary pyrite formation: an update. *Geochim. Cosmochim. Acta,* 48:605–615.

Canfield, D.E., 1989a. Reactive iron in marine sediments. *Geochim. Cosmochim. Acta,* 53:619–632.

————, 1989b. Sulfate reduction and oxic respiration in marine sediments: implications for organic carbon preservation in euxinic environments. *Deep-Sea Res. Part A,* 36:121–138.

————, 1991. Sulfate reduction in deep-sea sediments. *Am. J. Sci*., 291:177–188.

————, 1994. Factors influencing organic carbon preservation in marine sediments. *Chem. Geol.,* 114:315–329.

Canfield, D.E., Raiswell, R., and Bottrell, S., 1992. The reactivity of sedimentary iron minerals toward sulfide. *Am. J. Sci.,* 292:659–683.

Canfield, D.E., Raiswell, R., Westrich, J.T., Reaves, C.M., and Berner, R.A., 1986. The use of chromium reduction in the analysis of reduced inorganic sulfur in sediments and shale. *Chem. Geol.,* 54:149–155.

Chambers, L.A., and Trudinger, P.A., 1979. Microbiological fractionation of stable sulfur isotopes: a review and critique. *Geomicrobiol. J.,* 1:249–293.

Dromgoole, E.L., and Walter, L.M., 1990. Iron and manganese incorporation into calcite: effects of growth kinetics, temperature and solution chemistry. *Chem. Geol.*, 81:311–336.

Emerson, S., Jahnke, R., Bender, M., Froelich, P., Klinkhammer, G., Bowser, B., and Setlock, G., 1980. Early diagenesis in sediments from the Eastern Equatorial Pacific. I. Pore water nutrients and carbonate results. *Earth Planet. Sci. Lett.,* 49:57–80.

Froelich, P.N., Klinkhammer, G.P., Bender, M.L., Luedtke, N.A., Heath, G.R., Cullen, D., Dauphin, P., Hammond, D., Hartman, B., and Maynard, V., 1979. Early oxidation of organic matter in pelagic sediments of the eastern equatorial Atlantic: suboxic diagenesis. *Geochim. Cosmochim. Acta,* 43:1075–1090.

Gieskes, J.M., 1981. Deep-sea drilling interstitial water studies: implications for chemical alteration of the oceanic crust, layers I and II. *In* Warme, J.E., Douglas, R.G., and Winterer, E.L. (Eds.), *The Deep Sea Drilling Project: A Decade of Progress.* Spec. Publ.—Soc. Econ. Paleontol. Mineral., 32:149–167.

————, 1983. The chemistry of interstitial waters of deep-sea sediments: interpretation of deep-sea drilling data. *In* Riley, J.P., and Chester, R. (Eds.), *Chemical Oceanography* (Vol. 8): London (Academic), 221–269.

Gieskes, J.M., and Lawrence, J.R., 1981. Alteration of volcanic matter in deep-sea sediments: evidence from the chemical composition of interstitial waters from deep sea drilling cores. *Geochim. Cosmochim. Acta,* 45:1687–1703.

Gieskes, J.M., Schrag, D., Chan, L.-H., Zhang, L., and Murray, R.W., 1998. Geochemistry of interstitial waters. *In* Saunders, A.D., Larsen, H.C., and Wise, S.W., Jr. (Eds.), *Proc. ODP, Sci. Results,* 152: College Station, TX (Ocean Drilling Program), 293–305.

Henrichs, S.M., and Reeburgh, W.S., 1987. Anaerobic mineralization of marine sediment organic matter: rates and the role of anaerobic processes in the oceanic carbon economy. *J. Geomicrobiol.,* 5:191–237.

Iversen, N., and Jørgensen, B.B., 1993. Diffusion coefficients of sulfate and methane in marine sediments: influence of porosity. *Geochim. Cosmochim. Acta*, 57:571–578.

Kastner, M., and Gieskes, J.M., 1976. Interstitial water profiles and sites of diagenetic reactions, Leg 35, DSDP, Bellingshausen Abyssal Plain. *Earth Planet. Sci. Lett.,* 33:11–20.

Lasaga, A.C., and Holland, H.D., 1976. Mathematical aspects of non-steady state diagenesis. *Geochim. Cosmochim. Acta,* 40:257–266.

Lerman, A., 1975. Maintenance of steady state in oceanic sediments. *Am. J. Sci.,* 275:609–635.

Li, Y.-H., and Gregory, S., 1974. Diffusion of ions in seawater and deep sea sediments. *Geochim. Cosmochim. Acta,* 38:703–714.

Lyons, T.W., 1997. Sulfur isotopic trends and pathways of iron sulfide formation in upper Holocene sediments of the anoxic Black Sea. *Geochim. Cosmochim. Acta*, 61:3367–3382.

Lyons, T.W., and Berner, R.A., 1992. Carbon-sulfur-iron systematics of the uppermost deep-water sediments of the Black Sea. *Chem. Geol.*, 99:1–27.

Lyons, T.W., Werne, J.P., Hollander, D.J., Murray, R.W., Pearson, D.G., Peterson, L.C., and ODP Leg 165 Shipboard Scientific Party, 1998. Biogeochemical pathways in Holocene and latest Pleistocene sediments of the anoxic Cariaco Basin: Linkages to palaeoceanographic and palaeoclimatic variability. *Mineral. Mag*., 62A (part 2):931–932.

Machel, H.G., Krouse, H.R., and Sassen, R., 1995. Products and distinguishing criteria of bacterial and thermochemical sulfate reduction. *Appl. Geochem*., 10:373–389.

Martens, C.S., and Berner, R.A., 1974. Methane production in the interstitial waters of sulfate-depleted marine sediments. *Science*, 185:1167–1169.

McDuff, R.E., 1981. Major cation gradients in DSDP interstitial waters: the role of diffusive exchange between seawater and upper oceanic crust. *Geochim. Cosmochim. Acta,* 45:1705–1713.

McDuff, R.E., and Gieskes, J.M., 1976. Calcium and magnesium profiles in DSDP interstitial waters: diffusion or reaction? *Earth Planet. Sci. Lett.,* 33:1–10.

McGowran, B., 1989. Silica burp in the Eocene Ocean. *Geology,* 17:857–860.

Morse, J.W., and Mackenzie, F.T., 1990. *Geochemistry of Sedimentary Carbonates:* Amsterdam (Elsevier).

Müller, P.J., and Suess, E., 1979. Productivity, sedimentation rate, and sedimentary organic matter in the oceans, I. Organic carbon preservation. *Deep-Sea Res. Part A,* 26:1347–1362.

Ohmoto, H., 1972. Systematics of sulfur and carbon isotopes in hydrothermal ore deposits. *Econ. Geol.,* 67:551–579.

Raiswell, R., 1997. A geochemical framework for the application of stable sulphur isotopes to fossil pyritization. *J. Geol. Soc. London*, 154:343–356.

Raiswell, R., and Canfield, D.E., 1998. Sources of iron for pyrite formation in marine sediments. *Am. J. Sci*., 298:219–245.

Seyfried, W.E., Jr., and Bischoff, J.L., 1981. Experimental seawater-basalt interaction at 300°C and 500 bars: chemical exchange, secondary mineral formation, and implications for the transport of heavy metals. *Geochim. Cosmochim. Acta,* 45:135–147.

Shaw, T.J., and Meyers, P.A., 1996. The implications of turbidite-driven redox changes in sediments of the Iberia Abyssal Plain. *In* Whitmarsh, R.B., Sawyer, D.S., Klaus, A., and Masson, D.G. (Eds.), *Proc. ODP, Sci. Results,* 149: College Station, TX (Ocean Drilling Program), 301–304.

Shipboard Scientific Party, 1997a. Site 999. *In* Sigurdsson, H., Leckie, R.M., Acton, G.D., et al., *Proc. ODP, Init. Repts*., 165: College Station, TX (Ocean Drilling Program), 131–230.

Shipboard Scientific Party, 1997b. Site 1000. *In* Sigurdsson, H., Leckie, R.M., Acton, G.D., et al., *Proc. ODP, Init. Repts*., 165: College Station, TX (Ocean Drilling Program), 231–289.

Shipboard Scientific Party, 1997c. Site 1001. *In* Sigurdsson, H., Leckie, R.M., Acton, G.D., et al., *Proc. ODP, Init. Repts*., 165: College Station, TX (Ocean Drilling Program), 291–357.

Shipboard Scientific Party, 1997d. Site 1002. *In* Sigurdsson, H., Leckie, R.M., Acton, G.D., et al., *Proc. ODP, Init. Repts*., 165: College Station, TX (Ocean Drilling Program), 359–373.

Sigurdsson, H., Leckie, R.M., Acton, G.D., et al., 1997. *Proc. ODP, Init. Repts.,* 165: College Station, TX (Ocean Drilling Program).

Staudigel, H., and Hart, S.R., 1983. Alteration of basaltic glass: mechanisms and significance for the oceanic crust-seawater budget. *Geochim. Cosmochim. Acta,* 47:337–350.

Suess, E., 1980. Particulate organic carbon flux in the oceans: surface productivity and oxygen utilization. *Nature,* 288:260–263.

Thompson, G., 1983. Basalt-seawater interaction. *In* Rona, P.A., Boström, K., Laubier, L., and Smith, K.L., Jr. (Eds.), *Hydrothermal Processes at Seafloor Spreading Centers:* New York (Plenum), 225–278.

Toth, D.J., and Lerman, A., 1977. Organic matter reactivity and sedimentation rates in the ocean. *Am. J. Sci.,* 277:465–485.

Walter, L.M., and Burton, E.A., 1986. The effect of orthophosphate on carbonate mineral dissolution rates in seawater. *Chem. Geol.,* 56:313–323.

Date of initial receipt: 5 January 1999
Date of acceptance: 2 August 1999
Ms 165SR-020